Morphing shell structures: A refined, computationally-efficient solution of the governing equations

E. Lamacchia[1], A.Pirrera[1], I. V. Chenchiah[2] and P.M. Weaver[1]

[1]*Advanced Composites Centre for Innovation and Science, University of Bristol, Queen's Building, University Walk, Bristol BS8 1TR, UK*
[2]*School of Mathematics, University of Bristol, University Walk, Bristol BS8 1TW, UK*

Abstract

Morphing shells are nonlinear structures with the ability to change shape and adopt multiple stable states. By exploiting the concept of morphing, designers may devise adaptable structures, capable of accommodating a wide range of service conditions, minimising design complexity and cost.

At present, models predicting shell multistability are often a compromise between computational efficiency and result accuracy. This paper addresses the main challenges of describing the multistable behaviour of thin composite shells, such as bifurcation points and snap-through loads, through an accurate and computationally efficient energy-based method. The membrane and the bending components of the total strain energy are decoupled using the semi-inverse formulation of the constitutive equations. Transverse displacements are approximated by using Legendre polynomials and the membrane problem is solved in isolation by combining compatibility conditions and equilibrium equations. The result is the total strain energy as function of curvatures only. The minima of the energy with respect to the curvatures give the multiple stable configurations of the shell.

The accurate evaluation of the membrane energy is a key step in order to correctly capture the multiple configurations of the structure. Here the membrane problem is solved by adopting the Differential Quadrature Method (DQM), which provides accuracy of results at a relatively small computational cost.

Nomenclature

u, v	In-plane displacements
w	Transverse displacements
$2L_x, 2L_y$	Dimensions of the shell along the Cartesian axes
Ω	Surface area
$\boldsymbol{n}$	Vector normal to the surface Ω
h	Shell thickness
$\boldsymbol{\varepsilon}$	Green-Lagrange strain tensor
$\boldsymbol{\epsilon}$	Membrane strain tensor
$\boldsymbol{k}_0$	Curvature tensor of the undeformed configuration
$\boldsymbol{k}$	Curvature strain tensor of the deformed configuration
$\Delta\boldsymbol{k}$	Change in curvature from the undeformed to the deformed configuration
U_d, V_d, W_d	Coefficients used to scale the displacements
$\mathbf{E}$	Coefficients used to scale the in plane strains
$\mathbf{K}$	Coefficients used to scale the curvatures

$\boldsymbol{\sigma}$	Membrane stress tensor
$\boldsymbol{N}$	Membrane stress resultant
$\boldsymbol{\Sigma}$	Coefficients used to scale the membrane stress resultant
$\boldsymbol{M}$	Bending moment resultant
$\mathbf{Q}_k^*$	Lamina stiffness matrix
$\mathbf{A}$, $\mathbf{B}$, $\mathbf{D}$	In-plane, coupling and bending stiffness matrices respectively
Π	Total strain energy
Π_d	Coefficients used to scale the total strain energy
$\boldsymbol{\mathcal{L}}$	Differential operator
$\boldsymbol{\Sigma}_N$	Coefficients used to scale the thermoelastic stress resultant
$\boldsymbol{\Sigma}_M$	Coefficients used to scale the thermoelastic bending moment resultant
$\boldsymbol{\alpha}_k^*$	Secant thermal expansion coefficients of the lamina
T_0	Stress-free temperature
T_{ref}	Reference temperature
ΔT_0	Change in cure to room temperature
τ	Parameter used to characterise the thermal field
$P_l(\phi)$	Legendre polynomials
q_{ij}	Legendre parameters

Subscript

0	Undeformed reference surface
r	Inelastic deformation e.g. thermal, piezoelectric or moisture effects
k	Through the thickness position of the lamina

Superscript

$\sim$	Non-dimensional parameters

1 Introduction

Multistable structures may play an important role in future engineering designs due to their potential for reconfiguration between different states. Indeed, shape changing concepts may allow the designer to devise morphing structures able to adapt to a wide range of service conditions, minimising the design complexity.

A large variety of morphing concepts have been developed. These often utilise stiffness tailoring to provide shape changing features, such as non-symmetric composite plates or pre-stressed laminates [1–7].

However, non-linear models are often tailored for a specific case study, with a consequent limitation in describing, and adapting, to the large variety of morphing concepts present in literature. More general models, on the other hand, are often a compromise between computational efficiency and accuracy of results.

For example, the models proposed by Hyer [1] and Hamamoto et al. [8] assumed the laminate to be initially flat. Galletly et al. [9] and Guest et al. [10] relaxed this assumption, although restrictions on permissible constitutive equations or initial Gaussian curvatures still hold. In Eckstein et al. [11], an efficient Rayleigh-Ritz method able to describe the multi-mode morphing of a thermally-actuated initially cylindrical shell is presented, in which temperature-dependent material properties have been taken into account. Simple shape functions are employed to keep the computational cost to a minimum. For this reason, the inherent limitation of this model is the inability to accurately

describe the multistability of shells with general non-constant curvatures. Pirrera et al. [12] developed a shell model in which higher order polynomials are used to approximate the displacements. The large number of degrees of freedom due to the high order of the set of polynomials allows the restriction of a constant Gaussian curvature to be relaxed. However, the high order of the set of complete polynomials implied a large computational cost, thus loss of efficiency of the method.

Guest et al. [10] described the stability of a cylindrical shell with constant curvature by decoupling the contributions of the membrane and of the bending component of the total strain energy. Seffen [13] generalised this approach to elliptic planforms with constant curvature, whilst Vidoli [14] added quadratically varying curvature. Our approach builds upon these works by considering thin laminated shells possessing any non-constant curvature.

Although we consider structures that display shell-like behaviour, the mathematical assumptions behind the proposed model are the ones of initially curved plates. These assumptions are valid if the shell is sufficiently shallow, as shown by Mansfield in describing the bending behaviour of initially curved strips [15].

In the proposed model, the total strain energy is expressed as the sum of the stretching and curvature contributions. Once the problem is decoupled into the membrane and the bending components, one can solve an auxiliary set of membrane problems combining the membrane equilibrium equations and the constitutive equation, which links strains and curvatures according to Gauss' Theorema Egregium. This system of equations results in a strain field which is a function of the curvatures. By substituting the strain field into the stretching energy, one obtains an expression of the total strain energy which is now a function of the curvatures only. Finally, the Hessian of the total strain energy with respect to the curvatures evaluates the stability scenario.

By assuming constant curvature over the surface, Seffen [13] gave the closed form solution of the membrane strains for an elliptic planform. He solved the compatibility condition in terms of the Airy stress function by expressing the membrane stress as a second order polynomial, which upholds the boundary conditions of zero force and zero shear normal and tangent to the free boundary. Vidoli [14] relaxed the assumption of constant curvature over the surface, but he also observed that the limitation given by solving a series of auxiliary elliptic problems still holds, since the boundary conditions are satisfied exactly only for special geometries, i.e. shells with elliptic planforms or shells with lenticular cross section, as illustrated in Mansfield [15].

The investigation of a membrane problem with more general geometries calls for a numerical solution, as suggested in Vidoli and Maurini [16]. Following this observation, the present work solves the membrane problem by adopting an accurate and computationally efficient numerical method i.e. the Differential Quadrature Method (DQM). Moreover, the DQM allows the boundary conditions to be imposed in a point-wise fashion, whereas in Vidoli [14] are satisfied only in an average sense.

DQM was introduced by Bellaman and Casti [17] and it is based on the assumption that any continuous function can be approximated by a high-order polynomial in the overall domain, and that the derivative of a function can be expressed as a linear combination of the functional values at all the mesh points of the domain. Owing to the higher-order polynomial approximation, DQM usually requires fewer degrees of freedom in comparison to other approximation methods, such as Finite Element Method (FEM) or Finite Difference Method (FDM), to achieve accurate results [18].

The accuracy of the numerical method adopted to solve the membrane problem is crucial in order to evaluate the importance of each term in the energy functional. Other approximation methods, as polynomial expansions for the in-plane displacement fields, leads to loss of efficiency, as shown in Mattioni et al. [19], Aimmanee et al. [20] and Pirrera et al. [7]. In this sense, DQM guarantees accuracy at lower computational cost.

In Section 2 and Section 3 of this paper, we illustrate the general model and its non-dimensional form. By validating the model against available benchmark results in Section 4, we also show the

advantages of the proposed model compared to the ones present in literature. These advantages are summarized as follows:

- *Accuracy of results*: The transverse displacements have been approximated by using Legendre polynomials. This assumption allows the membrane and the bending components of the total strain energy to be accurately captured, as opposed to results obtained by using low orders of complete polynomials [11].
- *Boundary conditions satisfied point-wise*: The in-plane equilibrium equations have been discretised by using the DQM. This method allows the boundary conditions to be satisfied in a point-wise fashion, as opposed to a weak form [14].
- *Computational efficiency*: The computational cost is kept at acceptably low levels since the membrane problem is solved by simply inverting a sparse matrix of DQM weighting coefficients. The efficiency of the proposed model is particularly evident from the ability to capture the snap-through load with greater accuracy and using fewer degrees of freedom compared to the solution found using standard polynomial basis function [7].

Finally, Section 5 concludes the paper.

2 Methodology

2.1 Kinematic Equations and Total Strain Energy

In a Cartesian reference system x-y-z, the strains are defined in the usual form as a non-linear combination of linear deformations [21]. Under the assumptions of small strains and moderate rotations, the non-linear deformations for thin shallow shells are fully described by the Föppl-Von Kármán formulation of the strain field $\boldsymbol{\varepsilon}$, defined as [22]:

$$\boldsymbol{\varepsilon} = \boldsymbol{\epsilon} + z\boldsymbol{k}, \tag{1}$$

where

$$\begin{bmatrix} \epsilon_{xx} \\ \epsilon_{yy} \\ \epsilon_{xy} \end{bmatrix} = \begin{bmatrix} \dfrac{\partial u}{\partial x} + \dfrac{1}{2}\left(\dfrac{\partial w}{\partial x}\right)^2 \\ \dfrac{\partial v}{\partial y} + \dfrac{1}{2}\left(\dfrac{\partial w}{\partial y}\right)^2 \\ \dfrac{1}{2}\left(\dfrac{\partial v}{\partial x} + \dfrac{\partial u}{\partial y} + \dfrac{\partial w}{\partial y}\dfrac{\partial w}{\partial x}\right) \end{bmatrix}, \quad \begin{bmatrix} k_{xx} \\ k_{yy} \\ k_{xy} \end{bmatrix} = \begin{bmatrix} -\dfrac{\partial^2 w}{\partial x^2} \\ -\dfrac{\partial^2 w}{\partial y^2} \\ -2\dfrac{\partial^2 w}{\partial x \partial y} \end{bmatrix}, \tag{2}$$

are the mid-plane strains and the curvatures respectively. Here u, v are the in-plane and w the transverse displacements.

The total potential energy is defined by using Claperyon's theorem [23] as:

$$\Pi = \int_{\Omega} \int_{-h/2}^{h/2} \frac{1}{2} \boldsymbol{\sigma}^{\top} \boldsymbol{\varepsilon} \, dz d\Omega, \tag{3}$$

where the stress tensor is:

$$\boldsymbol{\sigma} = \mathbf{Q}\left(\boldsymbol{\varepsilon} - \boldsymbol{\varepsilon}_r\right). \tag{4}$$

Here $\mathbf{Q}$ is the plate stiffness, Ω is the surface area and h is the plate thickness. The subscript r describes the contribution of any inelastic deformation as for example thermal, piezoelectric or moisture effects.

For a laminate plate, assuming $\mathbf{A}$, $\mathbf{B}$ and $\mathbf{D}$ to be the in-plane, coupling and bending stiffness matrices [22], and defining $\boldsymbol{N}_r$ and $\boldsymbol{M}_r$ as the in-plane stress and moment resultants of the inelastic deformations, the total strain energy is written as [24]:

$$\Pi = \int_{\Omega} \left(\frac{1}{2} \begin{bmatrix} \boldsymbol{\epsilon} \\ \Delta\boldsymbol{k} \end{bmatrix}^{\top} \begin{bmatrix} \mathbf{A} & \mathbf{B} \\ \mathbf{B} & \mathbf{D} \end{bmatrix} \begin{bmatrix} \boldsymbol{\epsilon} \\ \Delta\boldsymbol{k} \end{bmatrix} - \begin{bmatrix} \boldsymbol{N}_r \\ \boldsymbol{M}_r \end{bmatrix}^{\top} \begin{bmatrix} \boldsymbol{\epsilon} \\ \Delta\boldsymbol{k} \end{bmatrix} \right) d\Omega, \tag{5}$$

where $\Delta\boldsymbol{k} = \boldsymbol{k} - \boldsymbol{k}_0$ describes the change in curvature from the reference undeformed configuration, having curvature $\boldsymbol{k}_0$, to the current deformed configuration $\boldsymbol{k}$.

By substituting into equation (5) the semi-inverse formulation of the constitutive relations expressed as [24]:

$$\begin{bmatrix} \boldsymbol{\epsilon} \\ \boldsymbol{M} + \boldsymbol{M}_r \end{bmatrix} = \begin{bmatrix} \mathbf{A}^* & \mathbf{B}^* \\ -\mathbf{B}^{*\prime} & \mathbf{D}^* \end{bmatrix} \begin{bmatrix} \boldsymbol{N} + \boldsymbol{N}_r \\ \Delta\boldsymbol{k} \end{bmatrix}, \tag{6}$$

where $\mathbf{A}^* = \mathbf{A}^{-1}$, $\mathbf{B}^* = -\mathbf{A}^{-1}\mathbf{B}$ and $\mathbf{D}^* = \mathbf{D} - \mathbf{B}\mathbf{A}^{-1}\mathbf{B}$, and where $\boldsymbol{N}$ and $\boldsymbol{M}$ are the in-plane stress resultants and bending moments, the total strain energy becomes:

$$\Pi = \int_{\Omega} \frac{1}{2} \left(\begin{bmatrix} \boldsymbol{N} \\ \Delta\boldsymbol{k} \end{bmatrix}^{\top} \begin{bmatrix} \mathbf{A}^* & \mathbf{0} \\ \mathbf{0} & \mathbf{D}^* \end{bmatrix} \begin{bmatrix} \boldsymbol{N} \\ \Delta\boldsymbol{k} \end{bmatrix} - \begin{bmatrix} \boldsymbol{N}_r \\ 2\boldsymbol{M}_r \end{bmatrix}^{\top} \begin{bmatrix} \mathbf{A}^* & \mathbf{B}^* \\ \mathbf{0} & \mathbf{I} \end{bmatrix} \begin{bmatrix} \boldsymbol{N}_r \\ \Delta\boldsymbol{k} \end{bmatrix} \right) \mathrm{d}\Omega. \tag{7}$$

The semi-inverse formulation of the constitutive relations expressed in equation (6) allows the total strain energy to be decoupled into the membrane and bending components, since the stiffness matrix is now a diagonal matrix and the element of coupling is embodied in $\mathbf{D}^*$. In general, the membrane and bending effects in a shell are coupled via the initial curvatures. The effects of this geometrical coupling are shown in the translation of the neutral axis in the deformed shape. In fact, the neutral axis might no longer be in the middle of the shell after deformation, especially if the deformed shape is not symmetric with respect to it. However, if the shell is sufficiently shallow, it is possible to capture this effect by mean of the semi-inverse formulation of the constitutive equations. Hence, each point of the neutral axis in the deformed configuration can be expressed as a linear combination of stretching and bending contributions.

2.2 Membrane Component

2.2.1 Theorema Egregium and Equilibrium Equations

A generic Riemannian manifold is completely characterised by its first and second fundamental form [25]. The components of the first and second fundamental form are not independent since they satisfy the compatibility (or integrability) conditions. In two dimensions, this conditions reduce to three non-vanishing differential equations [26], i.e. Gauss' Theorema Egregium and the Codazzi-Mainardi equations. These equations can be obtained from the Riemann tensor recast for a two-dimensional space. Physically, the compatibility relations between strains and curvatures represent the conditions of uniqueness of the normal vector at each point of the surface.

In the adopted Cartesian reference system and assuming small strains and moderate rotations, the compatibility condition for a thin shell is:

$$\frac{\partial^2 \epsilon_{yy}}{\partial x^2} + \frac{\partial^2 \epsilon_{xx}}{\partial y^2} - 2\frac{\partial^2 \epsilon_{xy}}{\partial x \partial y} = \det\Delta\boldsymbol{k}. \tag{8}$$

Equation (8) links the in-plane variation of the strain field with the change in Gaussian curvature, given by the determinant of the curvature tensor.

Introducing the differential operator $\mathcal{L}_1$ defined as:

$$\mathcal{L}_1 = \left[\frac{\partial^2}{\partial y^2}, \frac{\partial^2}{\partial x^2}, -2\frac{\partial^2}{\partial xy^2} \right], \tag{9}$$

and the semi-inverse formulation of the membrane strains expressed as in equation (6), the compatibility condition in terms of membrane stress resultants and curvatures becomes:

$$\mathcal{L}_1 \left[\mathbf{A}^* \left(\boldsymbol{N} + \boldsymbol{N}_r \right) + \mathbf{B}^* \Delta \boldsymbol{k} \right] = \det \Delta \boldsymbol{k}. \tag{10}$$

The membrane equilibrium equations for a free-free plate are [22]:

$$\begin{cases} \dfrac{\partial N_x}{\partial x} + \dfrac{\partial N_{xy}}{\partial y} = 0, & \text{on } \Omega, \\ \dfrac{\partial N_{xy}}{\partial x} + \dfrac{\partial N_y}{\partial y} = 0, & \text{on } \Omega, \\ \boldsymbol{N} \cdot \boldsymbol{n} = 0, & \text{on } \partial\Omega, \end{cases} \tag{11}$$

where $\partial\Omega$ is the boundary of the plate and $\boldsymbol{n}$ its normal.

Introducing the differential operators $\boldsymbol{\mathcal{L}}_2$ and $\boldsymbol{\mathcal{L}}_3$ defined as:

$$\boldsymbol{\mathcal{L}}_2 = \begin{bmatrix} \dfrac{\partial}{\partial x} & 0 & 0 \\ 0 & 0 & \dfrac{\partial}{\partial x} \end{bmatrix}, \quad \boldsymbol{\mathcal{L}}_3 = \begin{bmatrix} 0 & 0 & \dfrac{\partial}{\partial y} \\ 0 & \dfrac{\partial}{\partial y} & 0 \end{bmatrix}, \tag{12}$$

the equilibrium equations are recast as:

$$\left(\boldsymbol{\mathcal{L}}_2 + \boldsymbol{\mathcal{L}}_3 \right) \boldsymbol{N} = 0. \tag{13}$$

2.2.2 Membrane Problem

Combining equation (10) and equation (13), the solution of the membrane problem in terms of stress resultants is given by:

$$\boldsymbol{\mathcal{L}} \boldsymbol{N} = \begin{bmatrix} \det \Delta \boldsymbol{k} - \mathcal{L}_1 \mathbf{A}^* \boldsymbol{N}_r - \mathcal{L}_1 \mathbf{B}^* \Delta \boldsymbol{k} \\ \mathbf{0} \end{bmatrix}, \tag{14}$$

where the differential operator $\boldsymbol{\mathcal{L}}$ is defined as:

$$\boldsymbol{\mathcal{L}} = \begin{bmatrix} \mathcal{L}_1 \mathbf{A}^* \\ \boldsymbol{\mathcal{L}}_2 + \boldsymbol{\mathcal{L}}_3 \end{bmatrix}. \tag{15}$$

In order to solve equation (14), we discretise the matrix of differential operators defined in equation (15) by using the matrix formulation of DQM. A comprehensive description of the DQM in matrix form can be found in Lamacchia et al. [27]. By applying the DQM to equation (15), the differential operators $\mathcal{L}_1$, $\boldsymbol{\mathcal{L}}_2$ and $\boldsymbol{\mathcal{L}}_3$ become matrices of DQ weighting coefficients. The DQ weighting coefficients have been evaluated by following the approach presented by Shu [28]. In particular, the matrices of weighting coefficients for the first order derivatives in x and y have been evaluated by using Chebyshev polynomials, which have been shown to be numerically efficient and well behaved. The matrices of the higher order derivatives have been evaluated by using the recursive formula presented by Shu [28], which allows the weighting coefficients for the derivative of order n to be evaluated by simply applying n times the matrix multiplication rule to the weighting coefficients of the first order. Moreover, the Runge's phenomenon of oscillation at the edges of the domain [29] has been avoided by evaluating the DQ weighting coefficients on a Chebyshev-Gauss-Lobatto mesh grid [28, 30–32].

2.3 Equilibrium and Stability

In order to find a general curvature field that satisfies equation (14), the transverse displacements w have been approximated by using the Legendre polynomials defined as:

$$w(x,y) = w_0(x,y) + \sum_{i=0}^{n}\sum_{j=0}^{n} q_{ij} P_i(x) P_j(y), \tag{16}$$

where w_0 is the reference (undeformed) shell configuration and q_{ij} are the Legendre parameters. Here $P_i(x)$ and $P_j(y)$ are the shape functions of order n given by the Legendre polynomials and they are defined using binomial coefficients [33] as:

$$P_l(\phi) = \sum_{k=0}^{l} \binom{l}{k}\binom{-l-1}{k}\left(\frac{1-\phi}{2}\right)^k, \quad \text{for } l = i,j \text{ and } \phi = x,y. \tag{17}$$

Legendre polynomials are a complete set of orthogonal functions which have been shown to provide great robustness of results [34], both in terms of accuracy and flexibility to describe the deformed shape of the laminate. For each value of n, w is a $2n$ order polynomial in x and y. Hence we approximate w with $(n+1)^2$ degrees of freedom, i.e. all the distinct combinations of the i and j indices of the q_{ij} parameters, from 0 to n.

Equation (14) involves the solution of a set of independent membrane problems whose number depends on the order n of the Legendre polynomial. In particular, for $n = 1, 2, 3, 4, ...$, one needs to solve $2, 17, 80, 233, ...$ independent membrane problems respectively.

The differential operator $\boldsymbol{\mathcal{L}}$ takes into account also the boundary conditions. Hence, the matrix expressed in equation (15) is a rectangular matrix.

Finally, the in-plane stress resultants as function of curvatures only are obtained by solving equation (14):

$$\boldsymbol{N} = \boldsymbol{\mathcal{L}}^{-1}\begin{bmatrix} \det\Delta\boldsymbol{k} - \mathcal{L}_1\mathbf{A}^*\boldsymbol{N}_r - \mathcal{L}_1\mathbf{B}^*\Delta\boldsymbol{k} \\ \mathbf{0} \end{bmatrix}, \tag{18}$$

where $\boldsymbol{\mathcal{L}}^{-1}$ denotes the Moore-Penrose pseudo inverse of the differential operator $\boldsymbol{\mathcal{L}}$ [35, 36].

The in-plane stress resultants $\boldsymbol{N}$ of equation (18) are functions of the Legendre parameters q_{ij}. By substituting $\boldsymbol{N}$ in equation (7) we have an expression of the total strain energy as function of the q_{ij} only. The minima of the energy with respect to the q_{ij} give the equilibrium configurations:

$$\frac{\partial \Pi}{\partial q_{ij}} = 0. \tag{19}$$

The Hessian of the total potential energy with respect to the q_{ij} gives the stability positions:

$$\frac{\partial^2 \Pi}{\partial q_{ij}^2} > 0. \tag{20}$$

Finally, the stable or unstable configurations that the laminate assumes are given by substituting the q_{ij} obtained from equation (19) back into equation (16).

3 Non-dimensional Formulation

In order to reduce possible numerical ill-conditioning of the non-linear model and to analyse the relative importance of each term in the governing equations, the following non-dimensional

quantities are defined with the symbol *tilde* ($\tilde{}$):

$$\begin{array}{lll} x = L_x\tilde{x}, & y = L_y\tilde{y}, & \\ u = U_d\tilde{u}, & v = V_d\tilde{u}, & w = W_d\tilde{w}, \\ \boldsymbol{\epsilon} = \mathbf{E}\tilde{\boldsymbol{\epsilon}}, & \Delta\boldsymbol{k} = \mathbf{K}\Delta\tilde{\boldsymbol{k}}, & \boldsymbol{N} = \boldsymbol{\Sigma}\tilde{\boldsymbol{N}}. \end{array} \tag{21}$$

The dimensional parameters introduced in equation (21) are defined as:

- $2L_x$ and $2L_y$ are the dimensions of the plate along the Cartesian axes.
- U_d, V_d and W_d are coefficients used to scale the displacements [7, 37, 38] defined as:

$$\begin{aligned} U_d &= \tfrac{1}{L_x}\sqrt[2]{\mathbf{A}^*_{11}\mathbf{A}^*_{22}\mathbf{D}^*_{11}\mathbf{D}^*_{22}}, \\ V_d &= \tfrac{1}{L_y}\sqrt[2]{\mathbf{A}^*_{11}\mathbf{A}^*_{22}\mathbf{D}^*_{11}\mathbf{D}^*_{22}}, \\ W_d &= \sqrt[4]{\mathbf{A}^*_{11}\mathbf{A}^*_{22}\mathbf{D}^*_{11}\mathbf{D}^*_{22}}, \end{aligned} \tag{22}$$

  where $\mathbf{A}^*$ and $\mathbf{D}^*$ are in-plane compliance and reduced bending stiffness terms, respectively [24].

- $\mathbf{E}$ and $\mathbf{K}$ are used to scale the in plane strains and curvatures respectively and are defined as:

$$\mathbf{E} = \begin{bmatrix} \frac{1}{2}\frac{W_d^2}{L_x^2} & 0 & 0 \\ 0 & \frac{1}{2}\frac{W_d^2}{L_y^2} & 0 \\ 0 & 0 & \frac{W_d^2}{L_xL_y} \end{bmatrix}, \quad \mathbf{K} = \begin{bmatrix} -\frac{W_d}{L_x^2} & 0 & 0 \\ 0 & -\frac{W_d}{L_y^2} & 0 \\ 0 & 0 & -2\frac{W_d}{L_xL_y} \end{bmatrix}. \tag{23}$$

- $\boldsymbol{\Sigma}$ scales the membrane stress resultant $\boldsymbol{N}$ and it is defined as $\boldsymbol{\Sigma} = \mathbf{AE}$.

For sake of simplicity, let us consider the presence of a thermoelastic field as the inelastic contributions in the total strain energy. We define the thermoelastic in plane stress resultants and bending moments as:

$$\boldsymbol{N}_r = \boldsymbol{\Sigma}_N\tilde{\tau} \quad \text{and} \quad \boldsymbol{M}_r = \boldsymbol{\Sigma}_M\tilde{\tau}, \tag{24}$$

respectively, where

$$\begin{aligned} \boldsymbol{\Sigma}_N &= \sum_{k=1}^{\mathrm{N_{ply}}} \int_{z_k}^{z_{k+1}} \mathbf{Q}^*_k(T)\,\boldsymbol{\alpha}^*_k(T)\,\Delta T_0 dz, \\ \boldsymbol{\Sigma}_M &= \sum_{k=1}^{\mathrm{N_{ply}}} \int_{z_k}^{z_{k+1}} \mathbf{Q}^*_k(T)\,\boldsymbol{\alpha}^*_k(T)\,\Delta T_0 z dz, \end{aligned} \tag{25}$$

in which $\mathbf{Q}^*_k(T)$ and $\boldsymbol{\alpha}^*_k(T)$ are the laminate reduced stiffness matrix and the coefficients of thermal expansion respectively and they are both functions of the temperature. Moreover, $\Delta T_0 = T - T_{\mathrm{ref}}$ is the thermal gradient from cure temperature to room temperature and $\tilde{\tau}$ is a non-dimensional parameter defined as:

$$\Delta T_0\tilde{\tau} = T - T_{\mathrm{ref}}.$$

Substituting the parameters defined in equation (21) and (25) into equation (7), the non-dimensional form of the total strain energy is:

$$\tilde{\Pi} = \int_{-1}^{1}\int_{-1}^{1} \left[\frac{1}{2}\tilde{\boldsymbol{N}}^{\top}\tilde{\mathbf{A}}^{*}\tilde{\boldsymbol{N}} + \frac{1}{2}\Delta\tilde{\boldsymbol{k}}^{\top}\tilde{\mathbf{D}}^{*}\Delta\tilde{\boldsymbol{k}} - \frac{1}{2}\tilde{\tau}\tilde{A}_r^{*}\tilde{\tau} - \tilde{\tau}\tilde{\mathbf{b}}_r^{*}\Delta\tilde{\boldsymbol{k}} - \tilde{\tau}\tilde{\mathbf{d}}_r^{*}\Delta\tilde{\boldsymbol{k}}\right] \mathrm{d}\tilde{x}\mathrm{d}\tilde{y}, \tag{26}$$

where the non-dimensional matrices are defined as:

$$\begin{aligned}
\tilde{\mathbf{A}}^{*} &= \frac{L_x L_y}{\Pi_d}\boldsymbol{\Sigma}^{\top}\mathbf{A}^{*}\boldsymbol{\Sigma} = \frac{L_x L_y}{\Pi_d}\mathbf{E}\mathbf{A}\mathbf{E},\\
\tilde{A}_r^{*} &= \frac{L_x L_y}{\Pi_d}\boldsymbol{\Sigma}_N^{\top}\mathbf{A}^{*}\boldsymbol{\Sigma}_N,\\
\tilde{\mathbf{b}}_r^{*} &= \frac{L_x L_y}{\Pi_d}\boldsymbol{\Sigma}_N^{\top}\mathbf{B}^{*}\mathbf{K},\\
\tilde{\mathbf{D}}^{*} &= \frac{L_x L_y}{\Pi_d}\mathbf{K}^{\top}\mathbf{D}^{*}\mathbf{K},\\
\tilde{\mathbf{d}}_r^{*} &= \frac{L_x L_y}{\Pi_d}\boldsymbol{\Sigma}_M^{\top}\mathbf{K}.
\end{aligned} \tag{27}$$

The parameter Π_d is used to scale the total strain energy, so that $\Pi = \Pi_d\tilde{\Pi}$, where Π_d is defined as [7]:

$$\Pi_d = \mathrm{tr}\left(\begin{bmatrix}\mathbf{E} & \mathbf{0}\\ \mathbf{0} & \mathbf{K}\end{bmatrix}\begin{bmatrix}\mathbf{A} & \mathbf{B}\\ \mathbf{B} & \mathbf{D}\end{bmatrix}\begin{bmatrix}\mathbf{E} & \mathbf{0}\\ \mathbf{0} & \mathbf{K}\end{bmatrix}\right). \tag{28}$$

The compatibility condition expressed in equation (8) in terms of non-dimensional parameters is:

$$\frac{1}{2}\frac{\partial^2\tilde{\epsilon}_{xx}}{\partial\tilde{y}^2} + \frac{1}{2}\frac{\partial^2\tilde{\epsilon}_{yy}}{\partial\tilde{x}^2} - 2\frac{\partial^2\tilde{\epsilon}_{xy}}{\partial\tilde{x}\partial\tilde{y}} = \tilde{k}_{xx}\tilde{k}_{yy} - 4\tilde{k}_{xy}^2 - \left(\tilde{k}_{0xx}\tilde{k}_{0yy} - 4\tilde{k}_{0xy}^2\right). \tag{29}$$

Introducing the differential operator $\tilde{\mathcal{L}}_1$ defined as:

$$\tilde{\mathcal{L}}_1 = \frac{1}{2}\left[\frac{\partial^2}{\partial\tilde{y}^2}, \frac{\partial^2}{\partial\tilde{x}^2}, -4\frac{\partial^2}{\partial\tilde{x}\partial\tilde{y}}\right], \tag{30}$$

and the non-dimensional form of equation (6), equation (29) becomes:

$$\tilde{\mathcal{L}}_1\left(\tilde{\boldsymbol{N}} - \tilde{\mathbf{B}}^{*}\Delta\tilde{\boldsymbol{k}} + \boldsymbol{\Sigma}^{-1}\boldsymbol{\Sigma}_N\tilde{\tau}\right) = \tilde{k}_{xx}\tilde{k}_{yy} - 4\tilde{k}_{xy}^2 - \left(\tilde{k}_{0xx}\tilde{k}_{0yy} - 4\tilde{k}_{0xy}^2\right). \tag{31}$$

where

$$\tilde{\mathbf{B}}^{*} = \boldsymbol{\Sigma}^{-1}\mathbf{B}\mathbf{K}. \tag{32}$$

Similarly, the equilibrium conditions expressed in equation (13) becomes:

$$\frac{\sqrt{L_x L_y}}{\mathrm{tr}(\boldsymbol{\Sigma})}\left[\frac{1}{L_x}\tilde{\boldsymbol{\mathcal{L}}}_2\boldsymbol{\Sigma} + \frac{1}{L_y}\tilde{\boldsymbol{\mathcal{L}}}_3\boldsymbol{\Sigma}\right]\tilde{\boldsymbol{N}} = \mathbf{0}. \tag{33}$$

Finally, combining equation (31) and equation (33), the membrane problem is given by:

$$\begin{bmatrix} \tilde{\mathcal{L}}_1 \\ \dfrac{\sqrt{L_x L_y}}{\mathrm{tr}(\boldsymbol{\Sigma})}\left[\dfrac{1}{L_x}\tilde{\boldsymbol{\mathcal{L}}}_2 + \dfrac{1}{L_y}\tilde{\boldsymbol{\mathcal{L}}}_3\right]\boldsymbol{\Sigma} \end{bmatrix}\tilde{\boldsymbol{N}} = \begin{bmatrix} \tilde{\mathcal{L}}_1\tilde{\mathbf{B}}^{*}\Delta\tilde{\boldsymbol{k}} + \tilde{k}_{xx}\tilde{k}_{yy} - 4\tilde{k}_{xy}^2 - \left(\tilde{k}_{0xx}\tilde{k}_{0yy} - 4\tilde{k}_{0xy}^2\right) \\ \mathbf{0} \end{bmatrix}, \tag{34}$$

As already observed in Section 2, of great significance is that equation (34) gives the in-plane stress resultants $\tilde{\boldsymbol{N}}$ as functions of curvatures $\tilde{\boldsymbol{k}}$. Let us define

$$\tilde{\boldsymbol{\mathcal{L}}} = \begin{bmatrix} \tilde{\mathcal{L}}_1 \\ \dfrac{\sqrt{L_x L_y}}{\mathrm{tr}(\boldsymbol{\Sigma})} \left[\dfrac{1}{L_x} \tilde{\boldsymbol{\mathcal{L}}}_2 + \dfrac{1}{L_y} \tilde{\boldsymbol{\mathcal{L}}}_3 \right] \boldsymbol{\Sigma} \end{bmatrix}, \tag{35}$$

and

$$\boldsymbol{f} = \begin{bmatrix} \tilde{\mathcal{L}}_1 \tilde{\mathbf{B}}^* \tilde{\boldsymbol{k}} + \tilde{k}_{xx}\tilde{k}_{yy} - 4\tilde{k}_{xy}^2 - \left(\tilde{k}_{0xx}\tilde{k}_{0yy} - 4\tilde{k}_{0xy}^2 \right) \\ \mathbf{0} \end{bmatrix}. \tag{36}$$

The solution of the membrane problem is simply given by:

$$\tilde{\boldsymbol{N}} = \tilde{\boldsymbol{\mathcal{L}}}^{-1} \boldsymbol{f}, \tag{37}$$

which is a function of x, y and the curvature field $\Delta\tilde{\boldsymbol{k}}$.

Analogously to Section 2.3, by substituting equation (37) into equation (26) we obtain and expression of the total strain energy as function of the curvatures only. The equilibrium positions are obtained by minimising equation (26) with respect to the Legendre parameters.

It is interesting to observe that the operator expressed in equation (30) is a second order differential operator. Hence, in equation (31) the effects of any constant or linearly varying external field in x and y vanish. In other words, any external field contributes to the development of curvatures if and only if it is at least of the second order in x or y.

In order to visualise this property, we consider a constant and a quadratically-distributed thermal field applied to the cylindrical shell depicted in Figure 1a. For sake of simplicity, and to avoid any membrane-bending coupling due to stiffness properties, we consider an isotropic Aluminium (Al 6061-T6) shell, having in plane dimensions 1m×1m and thickness 0.005m. The initial curvature is $3\mathrm{m}^{-1}$ about the x axis. The magnitude of the applied thermal gradient is 100°C and the shell is clamped at the centre.

Figure 1b and Figure 1c show the deformations of the two orthogonal cross sections of the cylindrical shell represented by the blue and red lines in Figure 1a. In particular, Figure 1b shows that the originally curved cross section deforms both in-plane and out-of-plane independently of the distribution of the external thermal field. Conversely, by observing Figure 1c, it is evident that the originally flat cross section deforms just in-plane along the y axis under a constant external thermal load, whereas it deforms both in-plane and out-of-plane when a quadratically distributed thermal field is applied.

Hence, the Gaussian curvature of the deformed configuration does not change with respect to the reference configuration if the distribution of the external thermal field is constant (or linear) over the surface. Conversely, the initially cylindrical shell deforms by changing its Gaussian curvature to accommodate the inelastic stress if the external field is at least of the second order in x or y.

4 Validation

4.1 Case-Study 1: Multi-mode Morphing

In Eckstein et al. [11] the deformation of an initially cylindrically curved unsymmetric $[0_4/90_4]$ laminate under thermal loads is studied. The combination of initial curvature and opposite thermal moments was found to give rise to multiple deformation modes. The laminate shows two orthogonal bending modes at curing and room temperature, and an intermediate twisting mode.

The authors formulated a Rayleigh-Ritz analytical model assuming a second order polynomial to approximate the out of plane displacements, with a resulting constant curvature tensor as in

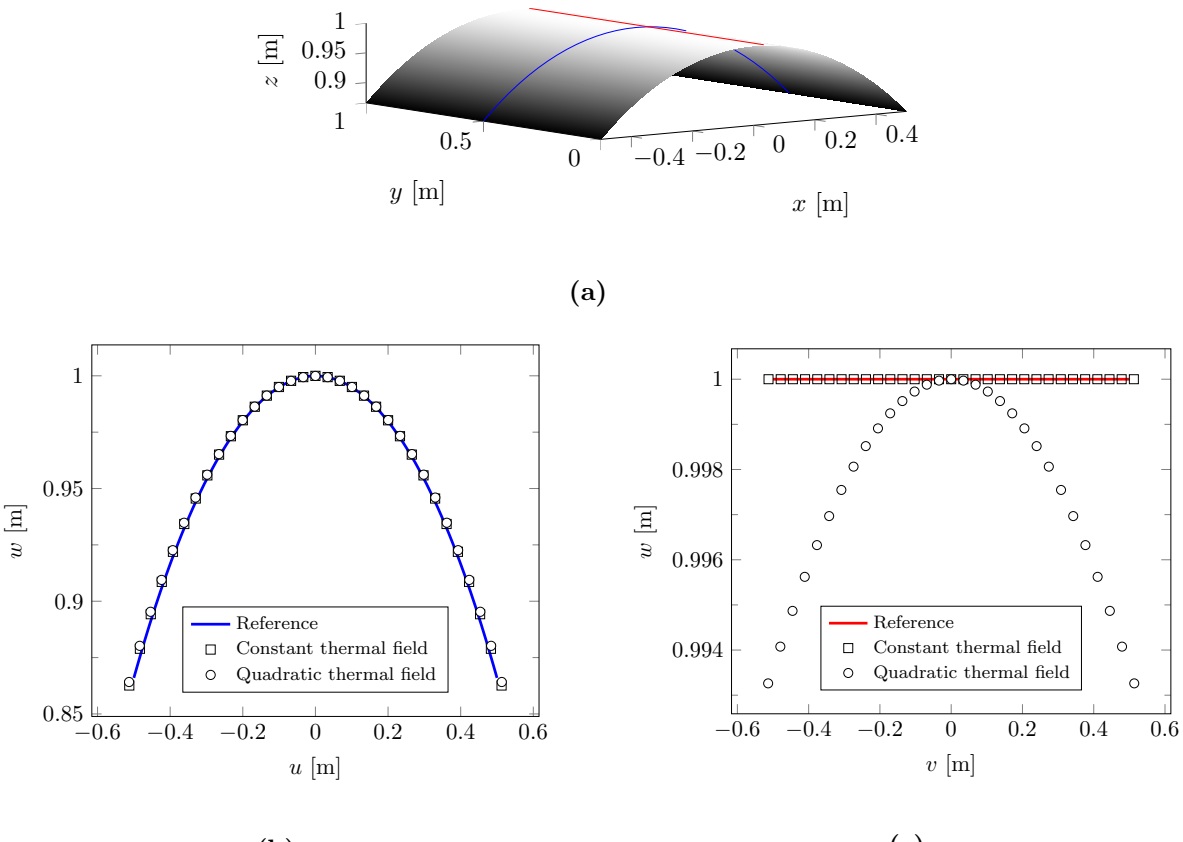

Figure 1: Figure 1c and Figure 1b show respectively the displacements of the initially curved cross section (blue line in Figure 1a) and of the initially flat cross section (red line in Figure 1a) due to a constant and quadratically-varying thermal field over the shell surface. From Figure 1c is evident that the initially flat cross section deforms just in-plane under a constant thermal load, whereas it deforms both in-plane and out-of-plane due to the quadratically-distributed thermal field over the shell surface. From Figure 1b is evident that the initially curved cross section deforms both in-plane and out-of-plane independently of the distribution of the thermal field. Here u, v and w are the displacements along y and z respectively.

Dano et al. [39]. The model was validated against a FEM simulation consisting of `256 ABAQUS S8R` elements, using a uniformly distributed mesh. The FEM and the Rayleigh-Ritz analytical model showed excellent agreement in predicting the two orthogonal cylindrical shapes. However, the analytical model overpredicted the values of curvatures in the range of temperatures when twisted configurations are present. The authors claimed that this limitation was due to the simple functions that were used to describe the in-plane strains, resulting in an overestimation of the membrane stiffness. This constraint makes it preferential for the laminate to store strain energy in the form of the bending component, hence the overprediction of the curvatures. The authors also observed that the approach adopted in Fernandes et al. [40] would likely yield more accurate results, because the membrane problem is first approximated with more degrees of freedom and then solved separately using a FEM. This model relies on the simplifying hypothesis of uniform curvature throughout the morphing process. Following the work done by Guest and Pellegrino [10], Seffen [13] and Seffen et al. [41], the global stability scenario can be described as function of curvature only.

As discussed in Section 1, the present work follows a similar approach. Hence, the multi-mode morphing presented in Eckstein et al. [11] is used to validate our model and eventually show further insight. In particular, in this section we show the benefits provided by the Legendre polynomials in accurately capturing the membrane and the bending component of the total strain energy compared to lower order basis functions. This choice results in the correct estimation of the membrane stiffness as opposed to adopting second order polynomials [11].

For the sake of simplicity, we have adapted the work done in Eckstein et al. [11] by considering material properties which are constant with the temperature as reported in Table 1. Shell dimensions and curvatures have remained unchanged from reference [11]. A FE analysis has been performed by using ABAQUS, a commercially available software for non-linear analysis. The shell is modelled using `8100 S4R` elements with a total of 8281 nodes, which provides convergence of results. The cooling-down process has been simulated by using both `Static-General` and `Riks` steps with `Nlgeom` on. An imperfection in the form of a corner force has been introduced in order to drive the deformation towards the stable twisted configuration. The effect of the imperfection is negligible since the shell assumes a cylindrical (non-twisted) configuration outside the bifurcation region. In order to achieve convergence, it has been necessary to introduce numerical dissipation [12]. The `dissipation factor` has been chosen to be sufficiently small so that the ratio between dissipated energy and total strain energy was always below 1E-03.

Figure 2 shows the convergence of results given by the proposed model in terms of the order n of the Legendre polynomials compared to the FE analysis. Note that the convergence in terms of number of nodes has been reached by using a Chebyshev-Gauss-Lobatto mesh grid consisting of $31\times$ 31. Figure 2 shows the displacements of two adjacent corners of the shell as function of temperature. The shell is initially cylindrical in its stress free configuration at 180°C. During the cooling down process, the shell approaches the first bifurcation point at 124°C when the twisted configuration appears. The shell remains in its twisted configuration until the second bifurcation point at 54°C when a new cylindrical configuration appears, orthogonal to the initial one. By decreasing the temperature up to 0°C, the shell keeps its cylindrical configuration and no further bifurcation points are present. Convergence has been reached by using the sixth order of the Legendre polynomials. Results for $n = 6$ are in excellent agreement with FE `Static-General`. Is it interesting to observe that the FE simulation performed using `Riks` was unable to capture the stable twisted configurations, despite the presence of the imperfection. Conversely, the analysis carried out using `Static-General` steps describes perfectly the twisted behaviour, although without net bifurcation points, as it is clear from the insets of Figure 2.

As already observed, the shape functions used in Eckstein et al. [11] describe accurately the cylindrical shapes. However, they revealed to be not flexible enough to accurately describe the twisted deformations. Hence the overestimation of the values of curvature for the range of temper-

Table 1: Material properties for the unsymmetric $[0_4/90_4]$ laminate.

E_{11} [GPa]	E_{22} [GPa]	G_{12} [GPa]	ν_{12} [−]	α_{11} [10^{-6}/°C]	α_{22} [10^{-6}/°C]
129.55	8.85	5.28	0.33	-2.26	23.4

ature where the twisted configurations are expected. Conversely, the use of Legendre polynomials in the present model are able to describe accurately the deformed shapes for all the values of temperature considered, with a significant improvement of accuracy compared to reference [11] .

The accuracy of the Legendre polynomial in capturing the deformed shapes is shown in Figure 3. The colour maps plotted onto the deformed shells represent the norm of the error between the displacements obtained by using the FEM `Static-General` and the order 6 of the Legendre polynomials, for the three characteristic configurations at 0°C, 90°C and 180°C. The norm of the error on the displacement field is defined in percentage as:

$$\|e\| = \frac{\int_0^{2L_x}\int_0^{2L_y}\sqrt{(u_{\text{FE}}-u_{\text{Leg.}})^2+(v_{\text{FE}}-v_{\text{Leg.}})^2+(w_{\text{FE}}-w_{\text{Leg.}})^2}\text{d}x\text{d}y}{\int_0^{2L_x}\int_0^{2L_y}\sqrt{u_{\text{FE}}^2+v_{\text{FE}}^2+w_{\text{FE}}^2}\text{d}x\text{d}y}\times 100. \tag{38}$$

The largest difference in terms of displacements is ∼0.22%, localised at the edges of the shell and any further increments of n do not lead to any significant improvement of results.

4.2 Case-Study 2: Tristable Shell

In this section, the proposed model is validated against the work done by Vidoli [14] on a initially doubly-curved shell having layup $[45, -45, -45, 45, -45, 45, 45, -45]$ which provides a tristable behaviour. The shell has free-free boundary conditions, it is clamped in the middle and it has a 0.25 m × 0.25 m squared planform with a ply thickness of 0.125 mm.

As already mentioned in Section 1, the work done by Vidoli [14] investigates the tristable behaviour of a thin shell, assuming constant, linearly and quadratically-varying curvature over the surface. As stated from the author, the aim of this study is to provide an efficient tool for the qualitative analysis and the quick parametric study of multistable shells, with an intrinsic renounce to highly accurate results. The model is extremely efficient in terms of computational cost to capture the three stable configurations, using just two degrees of freedom. However, the low number of degrees of freedom allows the boundary conditions to be solved just on average, with a consequence loss of accuracy of results especially in the boundary layer regions. In this Section, while we validate the model against Vidoli [14], we also show how to satisfy point-wise the boundary conditions, keeping the computational cost at a relatively low level.

The proposed model has been validated against an FE simulation we performed using ABAQUS. The shell is modelled using `8100 S4R ABAQUS` elements with a total of 8281 nodes. The snapping from the undeformed configuration into the two deformed configurations has been modelled separately in two different simulations. In the first simulation, the shell deforms from the initial undeformed configuration, denoted as stable states 1 (SS1), into the second stable configuration denoted as stable state 2 (SS2). In the second simulation, the shell deforms from (SS1) to the stable state 3 (SS3). In each simulation, we set three `Static-General` steps, with `Nlgeom` on. In the first step, the predicted deformed shape (SS2 or SS3) has been imposed over SS1 in terms of displacements w. In the second step, the predicted displacements have been imposed just to the four middle points of each side of the shell, which is free to deform elsewhere. In the third step, no external displacements have been imposed, so that the shell is free to deform, finding its natural

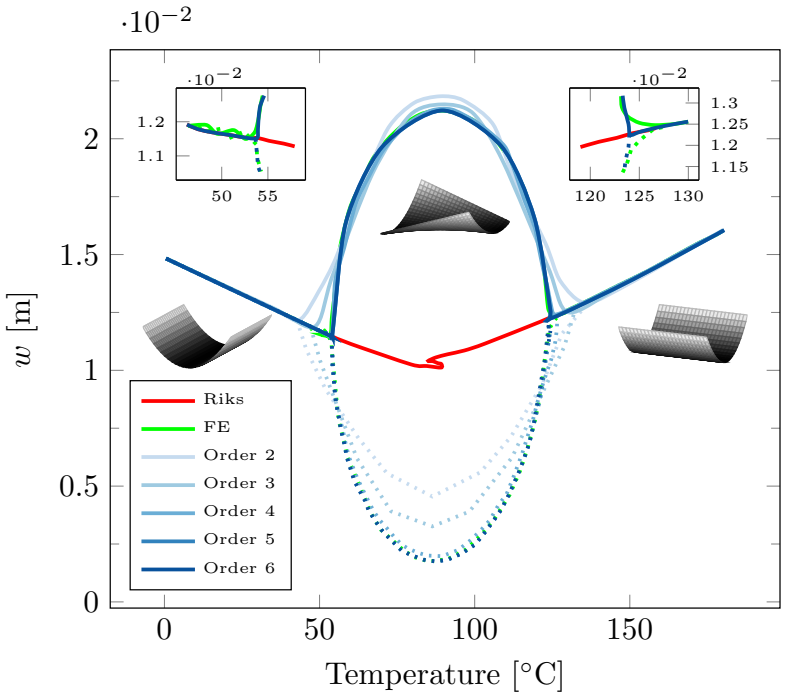

Figure 2: Displacements w of two adjacent corners of the cylindrical shell as function of temperature. The dotted and bold line in the figure correspond to any two adjacent corners of the shell. From cure temperature to the first bifurcation point at 124°C, the shell has a cylindrical configuration and any two adjacent corners displays the same out-of-plane displacement. In the region between the first bifurcation point and the second bifurcation point located at 54°C, the shell assumes a twisted configuration, hence two adjacent points display different out-of-plane displacements. By decreasing the temperature below the second bifurcation point, a new cylindrical configuration appears, orthogonal to the initial one. The Figure shows the convergence of the results given by the various order of the Legendre polynomials compared to the FE analysis. Results provided by using the sixth order of the Legendre polynomials ($n = 6$) are in excellent agreement with the FE, and any further increment of n does not lead to any significant improvement.

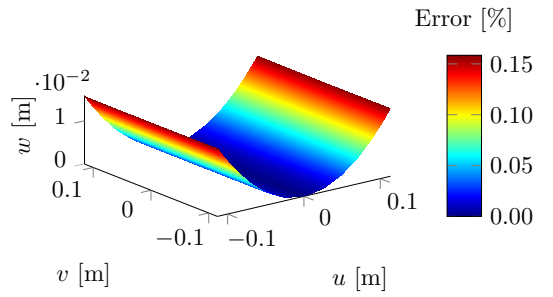

(a) Position error for the deformed shape at 0°C

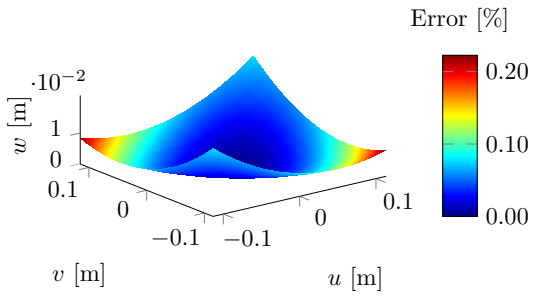

(b) Position error for the deformed shape at 90°C

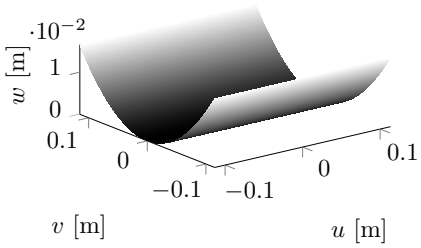

(c) Reference shape at 180°C

Figure 3: Difference in w between FE `Static-General` and the order 6 of the present model, for the three characteristic configurations at 0°C, 90°C and 180°C.

equilibrium configuration. This process avoids the need of introducing static dissipation to reach convergence, hence the FE simulations provides high accuracy and reliability of results.

Table 3 shows the out-of-plane displacement w of a corner of the shell as function of the order n of the Legendre polynomials. Results are in excellent agreement with FE and convergence is reached for n=5 and for a 29×29 Chebyshev-Gaus-Lobatto mesh grid.

In order to show the three stable configurations of the shell, in Figure 4 we present some of the results obtained using the second order Legendre polynomial ($n = 2$). The choice of using the solution given by n=2 allows the energy to be plotted against the only two non vanishing Legendre parameters q_{02} and q_{20}, which play the role of constant curvatures for $n = 2$. The contour plot of the energy shows three points of local minima, corresponding to the three stable configurations. This plot is similar to the one present in Vidoli et al. [16] for an initially doubly-curved shell.

In Figure 5, the three stable configurations obtained using the fifth order Legendre polynomials are shown. The contour plots reported onto each shape correspond to the difference in terms of displacements with respect to the FE simulation. Results are in excellent agreement, with a negligible difference of ∼0.8% at the corners of SS3. This order of accuracy is particularly due to the flexibility of the Legendre polynomial and to the boundary conditions solved point-wise. As already described in Section 2.2.2, the boundary conditions of zero force and zero shear normal and tangent to the edges of the shell need to be introduced in the differential operator $\tilde{\boldsymbol{\mathcal{L}}}$ expressed in equation (35). The differential operator $\tilde{\boldsymbol{\mathcal{L}}}$ is obtained by assembling the differential operators $\tilde{\boldsymbol{\mathcal{L}}}_1$, $\tilde{\boldsymbol{\mathcal{L}}}_2$ and $\tilde{\boldsymbol{\mathcal{L}}}_3$, and hence it is a $3\mathrm{N}^2 \times 3\mathrm{N}^2$ matrix containing the DQM weighting coefficients. Each edge of the shell upholds two boundary conditions, i.e. the normal and the shear stress resultants. Hence, eight equations have to be add to $\tilde{\boldsymbol{\mathcal{L}}}$, which becomes a rectangular matrix having dimensions $(3\mathrm{N}^2+8\mathrm{N})\times 3\mathrm{N}^2$. This guarantees the boundary conditions to be implemented in a point-wise fashion, with a negligible rise of the computational cost, since $\tilde{\boldsymbol{\mathcal{L}}}$ is a sparse matrix

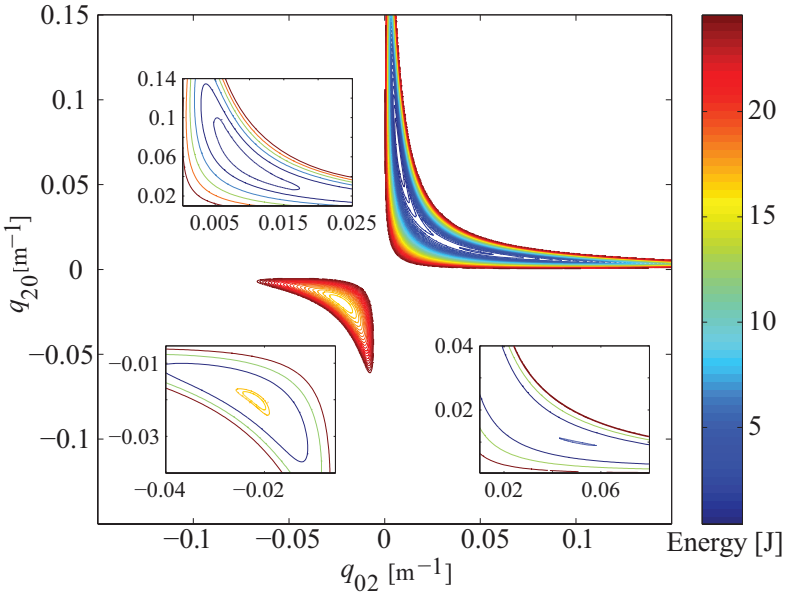

Figure 4: Contour plot of the total strain energy as function of the curvatures q_{02} and q_{20}. The insets show the three points of local minima, corresponding to the three stable states SS1, SS2 and SS3.

Table 3: Out-of-plane displacement w of a corner of the tristable shell as function of the order n of the Legendre polynomials.

Polynomial Order	SS1 w [m]	SS2 w [m]	SS3 w [m]
2	-0.1148	-0.08721	0.05533
3	-0.1148	-0.08725	0.05591
4	-0.1148	-0.08730	0.05623
5	-0.1148	-0.08731	0.05624
FE	-0.1148	-0.08732	0.05671

and the membrane stress resultants $\tilde{\boldsymbol{N}}$ are still obtained by simply pseudo-inverting $\tilde{\boldsymbol{\mathcal{L}}}$, as in equation (37).

Table 2: Material properties for the $[45, -45, -45, 45, -45, 45, 45, -45]$ laminate.

E_{11} [GPa]	E_{22} [GPa]	G_{12} [GPa]	ν_{12} [−]
207	5.17	2.59	0.25

4.3 Case-Study 3: Snap-Through Load

In this section, the proposed model is validated against the work done by Pirrera et al. [7] on the bistability of thin unsymmetric cylindrical plates. In particular, here we focus on the ability of our model in capturing the snap-through load in the bistable region. As illustrated in Diaconu et al. [42] and Pirrera and al. [7], a high number of degrees of freedom is necessary in order to accurately

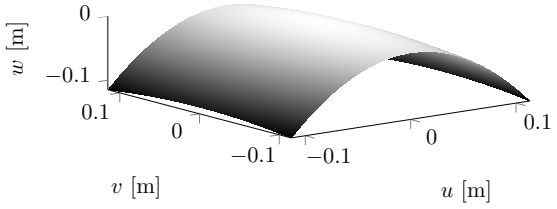

(a) Reference configuration SS1.

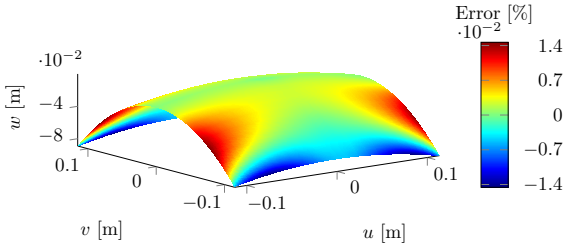

(b) Position error for SS2.

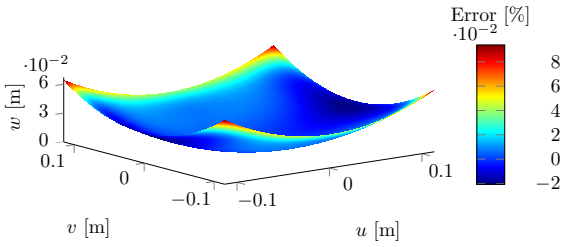

(c) Position error for SS3.

Figure 5: Difference in terms of displacements between FE `Static-General` and the order 5 of the present model, for the three stable states SS1, SS2 and SS3.

capture the value of the snap-through load, with a consequent loss of computational efficiency. In particular, in Pirrera et al. [7], it was necessary to increase the order of the set of complete polynomial approximation up to 11, corresponding to 62 degrees of freedom. This gives an error of just the 5% with respect to the results obtained from the FE model, used as benchmark. However, as stated from the authors, this level of accuracy required an extremely high computational cost, and any further increment of the order of the polynomial approximation was unfeasible.

Here we show the efficiency of our model in capturing the snap-through load for the thin unsymmetric $[0_2/90_2]$ plate proposed by Pirrera et al. [7]. Material properties are listed in Table 4. The plate is clamped in the middle node, it has a 0.25 m $\times$ 0.25 m squared planform and the ply thickness is 0.131 mm. Four corner forces have been applied along the z-axis, and equation (26) of the total potential energy is amended accordingly by adding the contribution of the external force. The cooling down process from curing to room temperature has been simulated by applying a thermal gradient of $\Delta T{=}{-}180°$C. The plate is initially flat and no external loads are applied. At room temperature, the plate is in its bistable region and an external load has been progressively applied up to the snapping point, where the unstable solution appears. The stability scenario has been evaluated through the Hessian of the energy with respect to the Legendre parameters. Figure 6 shows the force-displacements diagram at $\Delta T{=}{-}180°$C, corresponding to the region of bistability. The order of the Legendre polynomials has been increased up to convergence, as shown in Table 5. The insets of Figure 6 clearly shows that the solution given by $n{=}6$ (49 degrees of freedom) approaches the FE closer than the solution obtained in Pirrera et al. [7].

From this case study, the efficiency of the proposed model is particular evident, since the value of the snap-through load has been captured with greater accuracy and using fewer degrees of freedom compared to the solution found using standard polynomial basis functions [7].

Table 4: Material properties for the unsymmetric $[0_2/90_2]$ laminate.

E_{11} [GPa]	E_{22} [GPa]	G_{12} [GPa]	ν_{12} [−]	α_{11} [10^{-6}/°C]	α_{22} [10^{-6}/°C]
161	11.38	5.17	0.32	-1.8	3

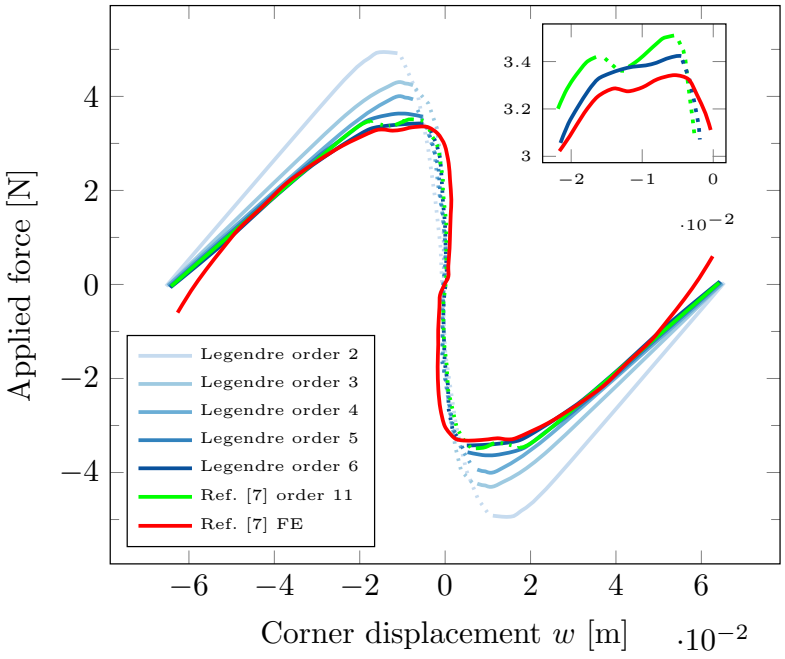

Figure 6: Force-displacement diagram at various approximation orders of the Legendre polynomial compared to the results of reference [7]. The comparison in proximity of the snapping load is reported in the insets. Solid and dotted lines represent the stable and the unstable solutions, respectively. The applied thermal gradient is ΔT=−180°C.

Table 5: Snapping load at various orders of Legendre polynomial compared with the results of reference [7].

Polynomial Order	Number of unknowns	Load [N]	Error [%]
Legendre 2	9	4.98	48.6
Legendre 3	16	4.32	28.9
Legendre 4	25	3.97	18.51
Legendre 5	36	3.65	8.96
Legendre 6	49	3.42	2.1
11, ref. [7]	62	3.51	5
FE, ref. [7]	15606	3.35	-

5 Conclusions

By exploiting anisotropy of composite materials along with the inherent geometric nonlinearity of curved shells, these structures display unique and interesting behaviours, including multistability and temperature-triggered shape-morphing capability. In this paper, we have presented a robust and accurate energy-based semi-analytical model to describe the multistable behavior of laminate shells for morphing applications. The key step of the proposed method is the decoupling of the total strain energy into the stretching and bending contributions.

The validation of the proposed model against available benchmark results showed how the correct evaluation of the membrane and bending components of the total strain energy influences the accuracy of the results. This accuracy has been achieved by using Legendre polynomials to approximate the transverse displacements and by discretising the membrane problem using the DQM. Moreover, the membrane stress resultants have been evaluated by simply inverting a sparse matrix of weighting coefficients. This operation keeps the computational cost to acceptably low levels and it allows the boundary conditions to be satisfied in a point-wise fashion.

The main advantages of the proposed model are summarised as follows:

- *Accuracy of results*: By using Legendre polynomials to approximate the transverse displacements, we have been able to capture accurately the values of the membrane and of the bending components of the total strain energy, as it is evident from the comparison with Eckstein et al. [11].

- *Boundary conditions satisfied point-wise*: The discretisation of the membrane problem using the DQM permits the satisfaction of the boundary conditions in a point-wise fashion, as opposed to a weak form [14].

- *Computational efficiency*: The membrane problem has been solved combining compatibility conditions and equilibrium equation. This keeps the computational cost at acceptably low levels since the resulting differential operator is a sparse matrix of DQ weighting coefficients. The efficiency is particularly evident from the ability to capture the snap-through load with greater accuracy and using fewer degrees of freedom compared to the solution found by using standard polynomial basis function [7].

References

[1] M. W. Hyer. Some observations on the cured shape of thin unsymmetric laminates. *Journal of Composite Materials*, 15:175–194, March 1981.

[2] S. Daynes, K. D. Potter, and P. M. Weaver. Bistable prestressed buckled laminates. *Composites Science and Technology*, 68(15–16):3431 – 3437, 2008.

[3] C. Thill, J. Etches, I. P. Bond, K. D. Potter, and P. M. Weaver. Morphing skins. *The Aeronautical Journal*, (112):117–139, 2008.

[4] C. G. Diaconu, P. M. Weaver, and F. Mattioni. Concepts for morphing airfoil sections using bi-stable laminated composite structures. *Thin-Walled Structures*, 46:689–701, 2008.

[5] S. Daynes and P. M. Weaver. A morphing composite air inlet with multiple stable shapes. *Journal of Intelligent Material Systems and Structures*, 22(9):961 – 973, 2011.

[6] Lachenal X., P. M. Weaver, and S. Daynes. Multistable composite twisting structure for morphing applications. *Proceedings of the Royal Society*, A 468:1230–1251, 2012.

[7] A. Pirrera, D. Avitabile, and P. M. Weaver. Bistable plates for morphing structures: a refined analytical approach with high-order polynomials. *International Journal of Solids and Structures*, 47(25-26):3412–3425, 2010.

[8] A. Hamamoto and M. Hyer. Non-linear temperature-curvature relationships for unsymmetric graphite-epoxy laminates. *International Journal of Solids and Structures*, 23:919–935, 1987.

[9] D. A. Galletly and S. D. Guest. Bistable composite slit tubes. ii. a shell model. *International Journal of Solids and Structures*, 462:4503–4516, 2004.

[10] S. D. Guest and S. Pellegrino. Analytical models for bistable cylindrical shells. *Proceedings of the Royal Society A: Mathematical, Physical and Engineering Science*, 462:839–854, 2006.

[11] E. Eckstein, A. Pirrera, and P. M. Weaver. Multi-mode morphing using initially curved composite plates. *Composite Structures*, 109:240–245, 2014.

[12] A. Pirrera, D. Avitabile, and P. M. Weaver. On the thermally induced bistability of composite cylindrical shells for morphing structures. *International Journal of Solids and Structures*, 49:685–700, 2012.

[13] K. A. Seffen. Morphing bistable orthotropic elliptical shallow shells. *Proceedings of the Royal Society A: Mathematical, Physical and Engineering Science*, 463:67–83, 2007.

[14] S. Vidoli. Discrete approximation of the Föppl-Von Kármán shell model: from coarse to more refined models. *International Journal of Solids and Structures*, 50:1241–1252, 2013.

[15] E. H. Mansfield. Bending, buckling and curling of a heated thin plate. *Proceedings of the Royal Society A: Mathematical, Physical and Engineering Science*, 268:316–327, 1962.

[16] S. Vidoli and C. Maurini. Tristability of thin orthotropic shells with uniform initial curvature. *Proceedings of the Royal Society A: Mathematical, Physical and Engineering Science*, 464:2949–2966, 2008.

[17] R. Bellman and J. Casti. Differential quadrature and long-term integration. *Journal of Mathematical Analysis and Applications*, 34(2):235–238, 1971.

[18] A. G. Striz, W. Chen, and C. W. Bert. Static analysis of structures by the quadrature element method (qem). *International Journal of Solids and Structures*, 2807(31), 1994.

[19] F. Mattioni, P. M. Weaver, and M. I. Friswell. Multistable composite plates with piecewise variation of lay-up in the planform. *International Journal of Solids Structures*, 46 (1):151–164, 2009.

[20] S. Aimmanee and M. W. Hyer. Analysis of the manufactured shape of rectangular thunder-type actuators. *Smart Materials and Structures*, 13(6):1389–1406, 2004.

[21] W. T. Koiter. On the nonlinear theory of thin elastic shells. *Proc. Koninklijke Nederlandse Akademie van Wetenschappen*, 38(B69):1–54, 1966.

[22] Reddy J.N. Mechanics of laminated composite plates and shells. *CRC PRess*, 2th ed., 2004.

[23] Love A.E.H. A treatise on the mathematical theory of elasticity. *Cambridge*, 4th ed.:173, 1927.

[24] E. H. Mansfield. The bending and stretching of plates. *Cambridge University Press*, Second edition, 1989.

[25] V. V. Novozhilov. The theory of thin shells - A translation by Lowe P.G. and Radok J.R.M. *P. Noordhoff LTD*, 1:27–29, 1959.

[26] A. J. McConnel. Application of the Absolute Differential Calculus. *Blackie and Son Limited*, 1:193–207, 1931.

[27] E. Lamacchia, A. Pirrera, I. V. Chenchiah, and P. M. Weaver. Non-axisymmetric bending of thin annular plates due to circumferentially distributed moments. *International Journal of Solids and Structures*, 51(3–4):622 – 632, 2014.

[28] C. Shu. Differential quadrature and its application in engineering. *Springer*, 2000.

[29] C. Runge. Über empirische funktionen und die interpolation zwischen äquidistanten ordinaten. *Zeitschrift für Mathematik und Physik*, 46:224–243, 1902.

[30] Embree M. and Trefethen L.N. Green's functions for multiply connected domains via conformal mapping. *SIAM Review*, 41:721–744, 1999.

[31] E. Hille. *Analytic Function Theory*, volume I. AMS Chelsea Publishing, 1962.

[32] Tsuji M. *Potential Theory in Modern Function Theory*. Dover Publications, 1959.

[33] W. Koepf. Hypergeometric summation: An algorithmic approach to summation and special function identities. *Braunschweig, Germany: Vieweg*, 1998.

[34] Z. Wu, G. Raju, and P.M. Weaver. Comparison of variational, differential quadrature, and approximate closed-form solution methods for buckling of highly flexurally anisotropic laminates. *Journal of Engineering Mechanics*, 139:1073–1083, 2012.

[35] E. H. Moore. On the reciprocal of the general algebraic matrix. *Bulletin of the American Mathematical Society*, 26 (9):394–395, 1920.

[36] R. Penrose. A generalized inverse for matrices. *Proceedings of the Cambridge Philosophical Society*, 51:406–413, 1955.

[37] C. G. Diaconu and P. M. Weaver. Postbuckling of long unsymmetrically laminated composite plates under axial compression. *International Journal of Solids and Structures*, 43(22–23):6978 – 6997, 2006.

[38] M. P. Nemeth. Nondimensional parameters and equations for nonliner and bifurcation analyses of thin anisotropic quasi-shallow shells. *NASA/TP-2010-216726*, pages 589–606, July 2010.

[39] M-L. Dano and M. W. Hyer. Thermally-induced deformation behavior of unsymmetric laminates. *International Journal of Solids and Structures*, 35:2101–2120, 1998.

[40] A. Fernandes, C. Maurini, and S. Vidoli. Multiparameter actuation for shape control of bistable composite plates. *International Journal of Solids and Structures*, 47:1449–1458, 2010.

[41] K. Seffen and R. McMahon. heating of a uniform wafer disk. *International Journal of Mechanical Science*, (49):230–238, 2007.

[42] C. G. Diaconu, P. M. Weaver, and A. F. Arietta. Dynamic analysis of bi-stable composite plates. *Journal of Sound and Vibration*, 322:987–1004, 2009.